UC Davis
UC Davis Previously Published Works

Title
Biogenic Manganese-Oxide Mineralization is Enhanced by an Oxidative Priming Mechanism for the Multi-Copper Oxidase, MnxEFG

Permalink
https://escholarship.org/uc/item/6m3972c7

Journal
Chemistry - A European Journal, 23(6)

ISSN
0947-6539

Authors
Tao, Lizhi
Simonov, Alexandr N
Romano, Christine A
et al.

Publication Date
2017-01-26

DOI
10.1002/chem.201603803

Peer reviewed

▌ Electrochemistry

Biogenic Manganese-Oxide Mineralization is Enhanced by an Oxidative Priming Mechanism for the Multi-Copper Oxidase, MnxEFG

Lizhi Tao[+],[a] Alexandr N. Simonov[+],[b, c] Christine A. Romano,[d] Cristina N. Butterfield,[d, e] Monika Fekete,[b] Bradley M. Tebo,[d] Alan M. Bond,[b] Leone Spiccia,*[b, c] Lisandra L. Martin,*[b] and William H. Casey*[a]

Abstract: In a natural geochemical cycle, manganese-oxide minerals (MnO_x) are principally formed through a microbial process, where a putative multicopper oxidase MnxG plays an essential role. Recent success in isolating the approximately 230 kDa, enzymatically active MnxEFG protein complex, has advanced our understanding of biogenic MnO_x mineralization. Here, the kinetics of MnO_x formation catalyzed by MnxEFG are examined using a quartz crystal microbalance (QCM), and the first electrochemical characterization of the MnxEFG complex is reported using Fourier transformed alternating current voltammetry. The voltammetric studies undertaken using near-neutral solutions (pH 7.8) establish the apparent reversible potentials for the Type 2 Cu sites in MnxEFG immobilized on a carboxy-terminated monolayer to be in the range 0.36–0.40 V versus a normal hydrogen electrode. Oxidative priming of the MnxEFG protein complex substantially enhances the enzymatic activity, as found by in situ electrochemical QCM analysis. The biogeochemical significance of this enzyme is clear, although the role of an oxidative priming of catalytic activity might be either an evolutionary advantage or an ancient relic of primordial existence.

Introduction

Manganese oxide minerals (MnO_x) are widely distributed over the Earth's surface[1] and their geochemical cycling is globally important. These minerals are among the most powerful natural oxidants in the environment where they efficiently degrade xenobiotic organic compounds to lower-molecular-mass compounds.[2] Manganese-oxide solids are also the terminal electron acceptors for dissimilatory metal-reducing bacteria in the oxidation of organic compounds or H_2 in the absence of oxygen.[2] Furthermore, MnO_x minerals can absorb and incorporate a wide range of metallic and non-metallic ions, such as lead,[3] cadmium,[4] arsenic,[5] chromium,[6] plutonium,[7] and uranium,[8] which contribute to regulatory mechanisms for the distribution and bioavailability of these elements in the environment. Overall, manganese-oxide minerals have been recognized as the "scavengers of the sea"[9] and are among the original classes of minerals that environmental chemists investigated.

In the photic zone of the ocean, MnO_x solids undergo reductive dissolution to soluble Mn^{2+}(aq). This process is counterbalanced by diurnal oxidation of Mn^{2+}(aq) back to the minerals,[10] where microorganisms (bacteria and fungi)[2, 11] are known to play an essential role. Biological oxidation of Mn^{2+} (aq) by molecular oxygen in seawater occurs at rates that are three to five orders of magnitude faster than abiotic pathways.[12] In a marine *Bacillus* species, one gene, *mnx*G encodes a putative multicopper oxidase[11b, 13] that has been identified as responsible for catalyzing the Mn^{2+}(aq) oxidation to MnO_x. The MnxG enzyme was recently isolated as part of a multiprotein complex where it is combined with several copies of accessory protein subunits: MnxE and MnxF.[11b, 14] The entire protein complex is denoted as MnxEFG and has a molecular weight of approximately 230 kDa.

[a] Dr. L. Tao,[+] Prof. W. H. Casey
Department of Chemistry and Department of Earth and Planetary Sciences
University of California, One Shields Avenue, Davis, California 95616 (USA)
E-mail: whcasey@ucdavis.edu

[b] Dr. A. N. Simonov,[+] Dr. M. Fekete, Prof. A. M. Bond, Prof. L. Spiccia, Assoc. Prof. L. L. Martin
School of Chemistry, Monash University, Victoria 3800 (Australia)
E-mail: leone.spiccia@monash.edu
        lisa.martin@monash.edu

[c] Dr. A. N. Simonov,[+] Prof. L. Spiccia
ARC Centre of Excellence for Electromaterials Science
Monash University, Victoria 3800 (Australia)

[d] Dr. C. A. Romano, Dr. C. N. Butterfield, Prof. B. M. Tebo
Division of Environmental and Biomolecular Systems
Institute of Environmental Health
Oregon Health & Science University
Portland, Oregon 97239 (USA)

[e] Dr. C. N. Butterfield
Current address: Department of Earth and Planetary Science
University of California Berkeley, Berkeley, California 94720 (USA)

[+] These authors contributed equally to this work.

📖 Supporting information for this article can be found under http://dx.doi.org/10.1002/chem.201603803.

The multicopper oxidase enzymes are a family of proteins found in bacteria, fungi, plants, and animals, and couple four sequential single-electron oxidations of substrates with four-electron reduction of O_2 to H_2O.[15] The well-studied examples are categorized into two groups based on the substrate. The first group use organic compounds as substrates and includes plant laccase, fungal laccase, ascorbate oxidase, and bilirubin oxidase.[15] The other group employ metal ions as substrates, such as Fet3p[16] and human ceruloplasmin,[16,17] which catalyze the oxidation of Fe^{II}, or the multicopper oxidase CueO that facilitates Cu^I oxidation during copper homeostasis in bacteria.[18] Interestingly, the capacity to catalyze $Mn^{2+}(aq)$ oxidation has been reported for CueO, CotA, and MnxG multicopper oxidases.[11b,14,19]

Currently, the enzymatically active MnxG protein cannot be purified without the MnxE and MnxF subunits, although the combined MnxEF subunits can be isolated separately from MnxG.[11b,14,19c] Previous studies[13,14] revealed that MnxG contains three types of redox-active copper sites, which are characteristic of multicopper oxidase enzymes.[15–17] These copper sites are referred to as Type 1 "blue" copper (T1Cu), Type 2 "normal" copper (T2Cu) and the "coupled binuclear" Type 3 copper (T3Cu), all of which are required for the oxidase activity. The mechanism of the enzymatic oxidation of organic compounds by O_2 in solution is well understood.[15] In these multicopper oxidases, the T1Cu site accepts electrons from the substrate and shuttles them by means of intramolecular electron transfer (with a rate constant of ca. 0.11 s^{-1} at 4 °C)[20] through a 13 Å long T1-Cys-His-T3 pathway to the trinuclear T2/3Cu site (consisting of one T2Cu and one binuclear T3Cu center).[15] In the trinuclear T2/3Cu site, exogenous O_2 is bound and rapidly reduced to water (with an apparent second-order rate constant of ca. 10^6 M^{-1} s^{-1}).[20,21] A similar mechanism is believed to apply to the MnxG-catalyzed aerobic oxidation of $Mn^{2+}(aq)$.[19c]

Previously, some of us employed electron paramagnetic resonance spectroscopy[19c] to study the kinetics of the $Mn^{2+}(aq)$ oxidation by molecular oxygen catalyzed by MnxEFG and probe the Mn^{II} binding states in the protein complex. In particular, it was established that there is a specifically bound mononuclear Mn^{II} that is coordinated to one nitrogenous ligand in the protein complex and a weakly exchanged–coupled dimeric Mn^{II} species.[19c] However, our understanding of the process of biogenic MnO_x mineralization by the newly discovered MnxEFG complex is still incomplete.

Electrochemical techniques offer a complementary highly useful strategy to study redox-active enzymes, including multicopper oxidases.[22] The capacity of the multicopper oxidases to efficiently catalyze electroreduction of molecular oxygen in neutral aqueous solutions has spurred recent research interest, specifically in the application as cathode catalysts in biofuel cells for implantable devices.[23] In these devices and in most contemporary bio-electrochemical studies, enzymes are integrated into the electrical circuit, typically through immobilization on a specific biocompatible electrode. Under properly designed conditions, T1Cu of a multicopper oxidase can accept electrons by means of direct electron transfer from the electrode rather than from a substrate, and then pass these elec-

trons through intramolecular electron transfer to the T2/3Cu sites, where O_2 is rapidly reduced to H_2O.

To date, the redox active sites of the MnxEFG protein complex and of the MnxG enzyme in particular, have not been probed by electrochemical methods. The present paper aims to fill this gap and reports on the first direct current (DC)- and Fourier transformed (FT) alternating current (AC) voltammetric[24] characterization of this MnO_x-producing enzyme. Adsorption of the MnxEFG enzyme directly on the electrode surface was monitored by quartz crystal microbalance (QCM) and its enzymatic activity was explored over a range of conditions.

Results and Discussion

The capacity to detect variations in mass down to 10 ng cm^{-2} by following changes in the frequency of an oscillating piezoelectric quartz sensor makes QCM a highly useful technique for biochemical research.[25] Changes in the QCM frequency (Δf) are proportional to the mass of the materials on the sensor surface, as given by the Sauerbrey equation: $\Delta m = -C\Delta f$, where C is a constant that reflects the physical properties of the crystal (ca. 18 ng cm^{-2} Hz^{-1} under our conditions) and Δf is the frequency change normalized to the QCM overtone number.[25] When the surface of a piezoelectric sensor is modified with a thin layer of an electric conductor (Au in our case), it can be used as a working electrode for electrochemical studies, in particular for probing electron-transfer mechanisms in redox proteins.[22f] Thus, coupling QCM with electrochemical techniques is an exceptionally powerful analytical tool, which has already proven its utility in many aspects of research.[26] The present work exploits major advantages of an electrochemical QCM to probe properties of MnxEFG and MnxEF during the catalytic reaction.

Initial experiments were undertaken to identify a surface that allows both immobilization of the proteins as well as a well-defined electrochemical response. Cyclic DC and FT AC voltammetry, as well as electrochemical impedance spectroscopy, were used for these experiments in a conventional electrochemical cell and were duplicated in a QCM chamber where possible (see the Experimental Section for the electrode platforms tested). Negatively charged surfaces were found to bind both MnxEFG and MnxEF with high affinity and can be conveniently prepared by self-assembly of mercaptohexanoic acid on a gold-sputtered SiO_2 crystal for QCM experiments (Stage **1** in Figure 1a). This surface immobilized the MnxEFG complex and the MnxEF subunit from dilute buffered solutions (Stage **2** in Figure 1a). Removal of weakly adsorbed species by washing the cell with protein-free solution yields a MnxEFG- or MnxEF-modified QCM sensor (Stage **3** in Figure 1a).

Figure 1b shows the $\Delta f - t$ QCM response during Stages **1–3** for MnxEFG and MnxEF. It was noted that Δf decreases (i.e., mass increases) as proteins are deposited (from Stage **1** to **2**) and then increases (i.e., mass decreases) as the protein-free buffer solution is flowed through the cell (from Stage **2** to **3**). The final concentration of the immobilized MnxEFG protein complex and MnxEF subunit was calculated as 0.6 ± 0.2 and 1.7 ± 0.3 pmol cm^{-2}, respectively. The resulting protein-
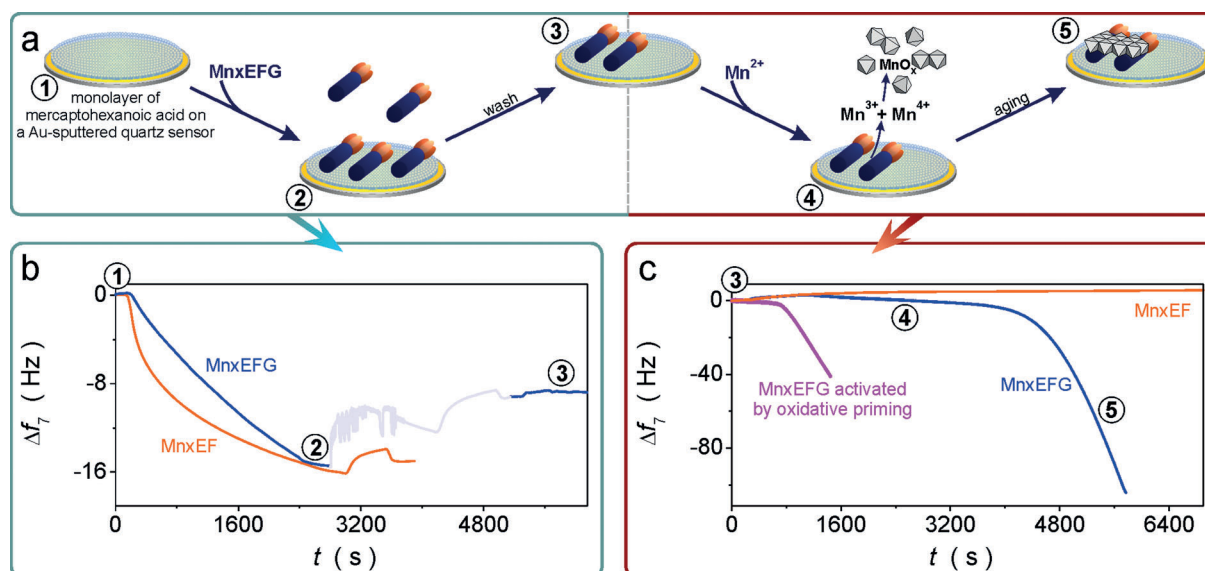
Figure 1. (a) Experimental steps for depositing and testing the enzymatic activity of the MnxEFG complex on the Au-sputtered quartz sensor modified with a monolayer of mercaptohexanoic acid. (b) Corresponding changes in QCM frequency during adsorption of the MnxEFG complex (blue) and the MnxEF subunit (orange) from Stage **1** to Stage **3** in (a). The less intensely colored curve shows the response from MnxEFG during electrochemical measurements shown in Figure 2. (c) MnO_x-mineralisation upon introduction of 0.4 mM Mn^{2+}(aq) (Stages **4** and **5** in (a)) is catalyzed by MnxEFG (blue), but not MnxEF (orange). The magenta curve shows enhancement in the activity of MnxEFG upon priming by electrooxidation at 0.85 V vs. NHE at Stage **3** in (a) prior to the introduction of manganese-containing solution. See the Experimental Section for details.

modified sensors were used for both electrochemical studies and catalytic experiments.

In situ QCM voltammetry

DC voltammograms obtained at Stages **1**–**3** of the QCM experiment (Figure 1 a) for adsorption of MnxEFG are shown in Figure 2. The reduction process (R1) and a poorly defined oxidation process (O1) are associated with the MnxEFG protein complex, because both signals decrease upon removal of dissolved MnxEFG from the cell (cf. voltammograms in Figure 2 at Stages **2** and **3**). The potential scan rate (v) dependence of the peak current (j_p) for R1 obtained in the presence (Stage **2**) and in the absence (Stage **3**) of the protein in solution is well approximated by a power law $j_p \approx v^{0.85 \pm 0.05}$. Although there is no peak detected for O1, the oxidative current at 0.6 V also demonstrates a similar dependence on the potential sweep rate ($j_p \approx v^{0.90 \pm 0.05}$). This is in acceptable agreement with the direct proportionality between j_p and v expected for a surface-confined process, which reinforces the conclusion that R1 and O1 are due to adsorbed protein.

However, it is unlikely that the DC voltammetric responses in Figure 2 a are due to metal-based redox transformations of the copper sites in the enzyme. Notably, this reduction process does not match, in either the shape or intensity, the broad oxidation response, as expected for a metal-based, surface-confined redox processes.[24d] The dissimilarities between the DC voltammetric R1 and O1 signals also indicate that the electron transfer processes are very slow. Moreover, using Faraday's law to convert the R1 and O1 charges to the surface concentration of adsorbed MnxEFG (assuming 10 $Cu^{2+/1+}$ sites per one
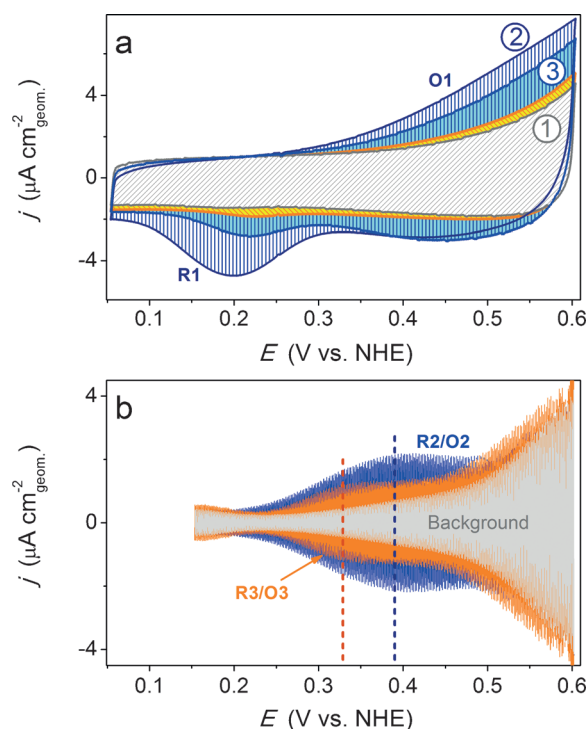

Figure 2. (a) DC voltammograms (scan rate, $v = 0.10$ V s^{-1}) obtained at Stages 1 (grey), 2 (MnxEFG = dark blue), and 3 (MnxEFG = blue; MnxEF = orange) of the QCM experiment shown in Figure 1 a. The hatched areas define charges associated with background current (grey), transformations of the adsorbed MnxEFG complex (dark blue and blue/cyan), and the MnxEF subunit (orange/yellow). (b) 3rd harmonic components of FT AC voltammograms ($f_{AC} = 9.02$ Hz; $\Delta E = 0.10$ V; $v = 0.03353$ V s^{-1}) obtained in a QCM cell at Stages 1 (grey) and 3 (MnxEFG = blue; MnxEF = orange) of the experiment. Dashed lines approximate E_{app} for R2/O2 (blue) and R3/O3 (orange).

MnxEFG protein complex)[11b] results in a value exceeding that derived from the QCM data by at least a factor of 3. The DC voltammogram for the MnxEF subunit is qualitatively similar to the MnxEFG, but with lower current densities for the protein-related processes. Taken together, these observations suggest that the voltammetric processes in Figure 2a have a minimal contribution from the copper sites of MnxEFG, but are dominated by unknown protein-based redox transformations.

Fortunately, the use of FT AC voltammetry (Figure S1 in the Supporting Information) can be used to probe fast electron-transfer events (as expected for the T1Cu and T2/3Cu sites) that are masked by either non-faradaic or slow faradaic processes in conventional DC voltammetry.[24b–d, 27] The basis of our FT AC voltammetry experiments is the analysis of non-linear, faradaic AC signal that is generated by a combination of a large-amplitude sinusoidal perturbation with frequency f_{AC} and a DC linear sweep (Figure S1). These components are detected as fundamental-, second-, and higher-order harmonics, that is, alternating current functions with frequencies f_{AC}, $2 f_{AC}$, and $n f_{AC}$ (n is the harmonic number), which together make up the total AC response. Each harmonic provides a different level of sensitivity to particular parameters of the system. For example, background current and very slow redox processes contribute to the fundamental components, whereas the third and higher-order harmonics are dominated by the faradaic response. These can be probed even at extremely low surface concentrations.[24c] Resolution of the total AC voltammetric signal into individual components is achieved by an FT-band selection/filtering–inverse FT sequence of operations, as explained in Figure S1.[24,27,28]

Comparison of the FT AC voltammetric data at Stages **1** and **3** of the QCM experiment (Figure 1a) reveals that chemically reversible faradaic signals develop within the 0.25–0.50 V range upon adsorption of both the MnxEFG complex (R2/O2; Figure 2b, blue) and the MnxEF subunit (R3/O3; Figure 2b, orange). These signals are superimposed upon a featureless background response (Figure 2b, grey) and are representative of electron-transfer processes expected for Cu$^{I/II}$ in the protein complex. The AC faradaic signal is distinguishable in the first four harmonic components, but is below the background (noise) level in higher AC harmonics (see Figures S1 and S2 in the Supporting Information). This suggests that the apparent rate of the Cu-based electron-transfer processes detected for the MnxEFG protein complex and the MnxEF subunit adsorbed on a carboxy-terminal monolayer is slow. This is most likely due to the bulky insulating protein structure inhibiting the direct electron transfer to the electrode.

For the MnxEF subunit, the R3/O3 AC voltammetric process in Figure 2b can be attributed to T2Cu$^{I/II}$, as there are only T2Cu sites in the MnxEF subunit.[14] Using the current maximum in the 3rd AC harmonic,[24d] the apparent reversible potential (E_{app}) for T2Cu$^{I/II}$ in the MnxEF subunit immobilized on a carboxy-terminated monolayer is estimated to be 0.33–0.35 V versus NHE (Figure 2b, orange dashed line). However, the MnxEFG protein with three different types of copper centers in the MnxG unit, as well as contributions from T2Cu centers of the MnxEF subunit, is more difficult to confidently assign. No-

tably, the AC signal associated with one of the Cu-sites of MnxG is detected within the same potential range (within 0.05 V more positive potential) than that assigned to the T2Cu of the MnxEF unit. Importantly, the reversible potentials, E_{app}, reported here might differ from the redox potentials of the active sites of proteins in solution. The effect of adsorption can distort such results and in order studies in which proteins are strongly adsorbed on an electrode surface. Indeed, enzyme binding to the surface might result in structural changes. However, the MnxEFG protein complex retains its enzymatic activity when immobilized on the MHA layer (see below), which suggests that no significant denaturation occurred upon adsorption.

Probing the MnxEFG and MnxEF electrochemistry at more positive potentials than those in Figure 2 was essentially impossible with the electrode platform employed. Attempts to probe potentials more positive than approximately 0.6 V gave rise to new intense DC and AC faradaic processes rapidly generated owing to the electrooxidation of the underlying MHA/Au support (Figure S2). These processes mask any responses from the proteins. Nevertheless, one feature that was apparent was a continuous positive shift of the DC voltammetric R1 process associated with MnxEFG upon oxidation (Figure S2).

Enzymatic activity: oxidative priming of MnxEFG

The enzymatic activity of the immobilized MnxEFG complex was assessed by following changes in the QCM frequency upon introduction of an air-saturated MnCl$_2$ solution (Figure 1c, blue trace). During the QCM experiments for the MnO$_x$ mineralization reported here, no external potential was applied to the sensor. Thus, the data in Figure 1c reflect the native-like enzymatic activity of the MnxEFG complex towards aerobic Mn^{2+}(aq) oxidation to produce solid MnO$_x$. After an induction period (Stage **4**, Figure 1c), a substantial decrease in Δf was observed, indicating an increase in mass due to the deposition of manganese-oxide solids on the QCM sensor. The deposited MnO$_x$ minerals are easily removed from the surface (from Stage **5** back to Stage **3**) by electrochemical reduction (Figure S3 in the Supporting Information).

The presence of MnO$_x$ at Stage **5** was further confirmed by scanning electron microscopy and elemental analysis, which also suggest that mineralization occurs predominantly at or near the MnxEFG complex. In Figure 3, a significantly higher amount of carbon in the area marked with a blue asterisk compared to the area marked with a red asterisk suggests a negligible concentration of the enzyme in the latter. A weak C EDX signal from the red asterisk area (Figure 3) could be from the mercaptohexanoic acid layer or unavoidable carbon-containing contaminants.

Preferential mineralization of MnO$_x$ on the protein surface is further supported by the overtone-dependent Δf–t response. This is exemplified in Figure 4, where different overtones demonstrate a more prominent decrease in Δf for the lower-order harmonics due to viscoelastic effects resulting from the deposition of "fuzzy" manganese oxide aggregates on the MnxEFG protein surface (see pages 87–88 in Ref. [25]).
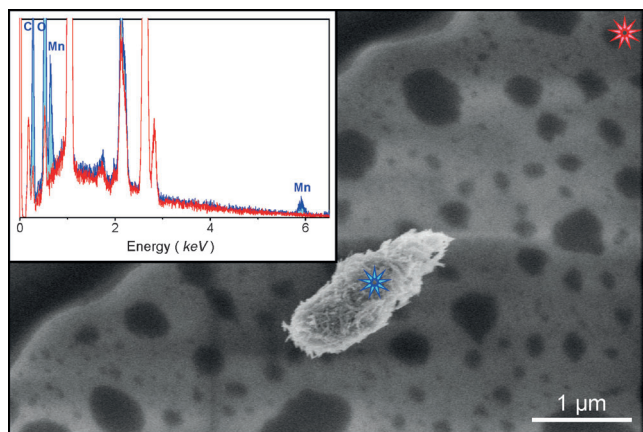
↖↖ These are not the final page numbers!

Figure 3. SEM image and local energy dispersive X-ray analysis of the biogenic MnO$_x$/MnxEFG aggregate (blue/turquoise) and the apparently enzyme-free area (red) on the Au-sputtered quartz sensor modified with a monolayer of mercaptohexanoic acid. Analysis was undertaken using a sensor dismounted from the QCM after Stage **5** of the experiment in Figure 1 a. Asterisks show the areas used for the EDX analysis.
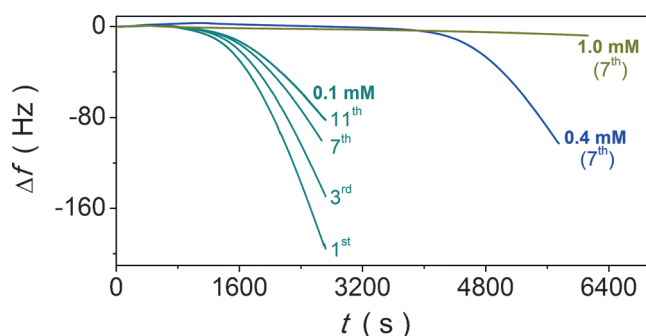

Figure 4. Mn^{2+}-concentration (c_{Mn}) dependence of the induction period for the MnxEFG-catalyzed mineralization of MnO$_x$ in QCM (Stage **5** of the experiment in Figure 1 a). $c_{Mn} = 0.1$ (teal), 0.4 (blue), and 1.0 mm (tan). For $c_{Mn} = 0.1$ mm, changes in Δf are shown for the 1st, 3rd, 7th, and 11th overtones, whereas only the 7th overtone is shown in other cases. All Δf data are shown normalized to the overtone number.

The QCM profiles for aerobic oxidation of Mn^{2+}(aq) to MnO$_x$-minerals, catalyzed by the MnxEFG protein complex, can be interpreted as follows. During the induction period (Stage **4** in Figure 1 c), manganous species in the MnxEFG protein complex are oxidized by dissolved O$_2$ to form Mn^{3+}/Mn^{4+} products, which are rapidly hydrolyzed and polymerized to generate insoluble MnO$_x$ particles. The molecular details of this step are unclear because the mass of generated MnO$_x$ is not detectable until the solution layer near the surface of QCM sensor is oversaturated. Then the MnO$_x$ minerals start to deposit on the QCM sensor at a rate of approximately 3.0×10^3–5.6×10^3 g of MnO$_x$ per mol of MnxEFG per second. Thus, the induction period reflects the enzymatic activity of MnxEFG protein complex in oxidizing Mn^{2+}(aq) using molecular oxygen.

Increasing the concentration of Mn^{2+} (c_{Mn}) clearly suppresses the MnxEFG-catalyzed biogenic mineralization of MnO$_x$ (Figure 4). This could arise from either substrate inhibition of the enzyme,[29] or possibly from a disproportionation reaction

(2 Mn^{III}⇌Mn^{II}+Mn^{IV}) during the initial stages of the MnO$_x$ mineralization, which is suppressed by additional manganous ions.

Importantly, the QCM results reveal the essential role of the multicopper oxidase MnxG unit within the MnxEFG complex for catalyzing the biogenic MnO$_x$ formation. Indeed, the immobilized MnxEF subunit itself exhibits no enzymatic activity (Figure 1 c, orange traces), illustrating that MnxEF alone is incapable of mineralizing Mn into MnO$_x$.

Most interestingly, the induction period is shortened by up to 80 % (Figure 1 c, magenta trace) when the immobilized MnxEFG complex is primed at Stage **3** by applying positive potentials of 0.85–0.90 V in situ to the protein-modified QCM sensor in contact with the Mn-free solution. We emphasize that no external potential was applied to the QCM sensor in the presence of Mn^{2+}(aq) and that MnO$_x$ mineralization in Figure 1 c is exclusively from enzymatic catalysis. Shortening of the induction period suggests that the activity of MnxEFG at Stage **4** is enhanced after oxidative priming, and the MnxEFG protein complex can generate MnO$_x$ at a faster rate near the surface of QCM sensor (Figure 1 c), which is followed by a similar deposition rate.

Difficulties in electrochemical analysis of copper sites of the MnxEFG protein complex immobilized on the MHA layer, especially at positive potentials, precluded us from probing the oxidative priming further. One possible reason is an irreversible conformational change of the protein induced by oxidation, which might be reflected by changes to the R1 voltammetric signal (Figure S2 in the Supporting Information).

The oxidative priming effect of the MnxEFG protein complex might be physiologically significant. Manganese oxides may be produced by microbial species as a protective layer to help withstand environmental stress.[30] From this perspective, the enhanced rate of the MnO$_x$ mineralization catalyzed by MnxEFG upon oxidative priming might reflect the natural self-protection mechanism of the cells against strong oxidants.

Conclusions

The present work reports the first electrochemical study of the Mn-oxidizing multicopper oxidase, MnxEFG from marine *Bacillus* species, which sustains one of the major enzymatic mechanisms for mineralization to form manganese-oxide solids. Under conventional DC voltammetric conditions, the interpretation of the data was complicated by protein-based faradaic processes that cannot be attributed to the enzymatic copper redox centers. However, analysis of the higher harmonic data of FT AC voltammograms allowed detection of faradaic processes with apparent reversible potentials of approximately 0.33–0.40 V versus NHE, which were tentatively attributed to the T2Cu sites in MnxEFG immobilized on a carboxy-terminated layer.

Catalytic QCM studies confirm that the enzymatic activity in the MnxEFG protein complex is due to the putative multicopper oxidase MnxG, whereas the role of the MnxEF is still to be established. Most interestingly, priming the MnxEFG protein complex by mild electrooxidation significantly enhances the catalytic activity of the MnxG enzyme towards aerobic Mn^{2+}

(aq) oxidation to produce MnO$_x$ minerals. This effect might have a physiological significance and be potentially useful for enhancing the biosynthetic capacity of the enzyme. It is probable that enzymatic activities of other multicopper oxidases can be enhanced following the same oxidative priming approach.

Experimental Section

Materials: The MnxEFG protein complex (*mnx*E$_3$F$_3$G, ca. 230 kDa) was obtained by expressing the *Bacillus* sp. PL-12 *mnx*DEFG operon in *E. coli* with or without a purification tag, using published procedures.[11b, 14] The MnxEF protein subunit was expressed from a plasmid encoding just the *mnx*E and *mnx*F genes and purified following the published procedure.[14]

Reagent- or analytical-grade chemicals were used as received from commercial suppliers. High-purity water (18 MΩ·cm; Sartorius Arium 611) was used in the preparation of all solutions and wherever water is mentioned. Prior to use, all glassware was soaked in H$_2$SO$_4$ (98 wt%):H$_2$O$_2$ (30 vol%) (1:1 vol) for at least 12 h, washed copiously with water and dried at 110 °C.

Quartz crystal microbalance: QCM measurements were conducted using a Q-sense E4 instrument (Q-Sense, Sweden) equipped with a QEC401 cell thermostated at 22 ± 1 °C and a quartz crystal sensor covered with a thin layer of gold metal (fundamental frequency 5 MHz; geometric area of gold-covered working surface 0.78 cm^2). An Ismatec peristaltic pump (ISM935; Switzerland) was used to introduce solutions into the cell.

Prior to use, quartz sensors were soaked in a H$_2$SO$_4$ (98 wt%):H$_2$O$_2$ (30 vol%) (1:1 vol) mixture for at least 24 h, washed copiously with water and isopropanol, and immersed in an isopropanol solution of 6-mercaptohexanoic acid (MHA; 1 mM) for at least 1 h. After modification with MHA, the sensors were gently rinsed with isopropanol, dried under nitrogen flow, and installed in the QCM cell. The changes in frequency (Δf) associated with the first, third, fifth, seventh, and ninth harmonics of the oscillating quartz sensor were recorded, but only data for the 7th harmonic are shown and discussed in the paper unless otherwise stated. All Δf data reported were normalized to the overtone number.

After a stable QCM response in water was achieved, an aqueous NaCl (500 mM) + HEPES (4-(2-hydroxyethyl)-1-piperazineethanesulfonic acid; 20 mM) solution (pH 7.8) was pumped (flow rate of 0.3 mL min^{-1}) through the cell until Δf stabilized. A solution (0.140 μM) of the MnxEFG protein complex or the MnxEF subunit in NaCl (500 mM) + HEPES (20 mM) (pH 7.8) was introduced to the QCM chamber at a flow rate of 0.05 mL min^{-1} over 30–50 min. Subsequent introduction of a protein free NaCl + HEPES solution pumped at 0.3 mL min^{-1} removed non-adsorbed proteins. For catalytic experiments, an aqueous solution of MnCl$_2$ (0.4 mM) in NaCl (500 mM) + HEPES (20 mM) (pH 7.8) was introduced (0.05 mL min^{-1} for 10 min) into the QCM chamber containing either MnxEFG- or MnxEF-modified sensors.

Voltammetric studies: These experiments were undertaken using either a BAS Epsilon electrochemical workstation or a custom-made FT AC voltammetry instrument[24a, 31] in a three-electrode configuration using a specialized electrochemical QCM attachment at 22 ± 1 °C. Electrochemical characterization was undertaken using air-saturated NaCl (500 mM) + HEPES (20 mM) (pH 7.8) electrolyte solutions.

The QCM sensor was used as a working electrode at different stages of the QCM experiment. The high-surface-area auxiliary Pt electrode and the reference AgCl-coated Ag electrode were immersed directly in the electrolyte solution under investigation. Use of this low-impedance reference system was necessary for high-quality AC voltammetric measurements. The potential of Ag | AgCl | NaCl (500 mM) + HEPES (20 mM) configuration did not vary significantly between experiments and was 0.057 ± 0.001 V versus Ag | AgCl | KCl(sat.) or 0.254 ± 0.001 V versus normal hydrogen electrode (NHE). All potentials are reported versus NHE and current densities are normalized to the geometric surface area of the electrode.

Preliminary electrochemical experiments used to determine a suitable immobilization strategy for the electroactive MnxEFG and MnxEF proteins were undertaken in a conventional Pyrex cell using the same reference and auxiliary electrode systems as the QCM cell. Apart from the MHA-modified Au, other electrodes tested were bare glassy carbon, bare Au, hexanethiol-modified Au, pyrolytic-graphite basal plane, pyrolytic-graphite edge plane (PGE) and PGE modified with co-adsorbents (either polymyxin B[32] or didodecyldimethylammonium bromide[33]). All were unsuitable for probing the redox properties of MnxEFG or MnxEF.

[1] J. E. Post, *Proc. Natl. Acad. Sci. USA* **1999**, *96*, 3447–3454.
[2] a) B. M. Tebo, J. R. Bargar, B. G. Clement, G. J. Dick, K. J. Murray, D. Parker, R. Verity, S. M. Webb, *Annu. Rev. Earth Planet. Sci.* **2004**, *32*, 287–328; b) T. G. Spiro, J. R. Bargar, G. Sposito, B. M. Tebo, *Acc. Chem. Res.* **2010**, *43*, 2–9.
[3] Y. M. Nelson, L. W. Lion, M. L. Shuler, W. C. Ghiorse, *Environ. Sci. Technol.* **1996**, *30*, 2027–2035.
[4] B. Müller, L. Granina, T. Schaller, A. Ulrich, B. Wehrli, *Environ. Sci. Technol.* **2002**, *36*, 411–420.
[5] M. Berg, H. C. Tran, T. C. Nguyen, H. V. Pham, R. Schertenleib, W. Giger, *Environ. Sci. Technol.* **2001**, *35*, 2621–2626.
[6] L. E. Eary, D. Rai, *Environ. Sci. Technol.* **1987**, *21*, 1187–1193.
[7] M. C. Duff, D. B. Hunter, I. R. Triay, P. M. Bertsch, D. T. Reed, S. R. Sutton, G. Shea-McCarthy, J. Kitten, P. Eng, S. J. Chipera, D. T. Vaniman, *Environ. Sci. Technol.* **1999**, *33*, 2163–2169.
[8] D. W. Kennedy, J. K. Fredrickson, J. M. Zachara, Y. A. Gorby, A. Dohnalkova, M. Duff, *Abstr. Gen. Meet. Am. Soc. Microbiol.* **2000**, *100*, 494.
[9] E. D. Goldberg, *J. Geol.* **1954**, *62*, 249–265.
[10] W. G. Sunda, S. A. Huntsman, *Deep-Sea Res. Part A* **1988**, *35*, 1297–1317.
[11] a) A. Soldatova, C. Butterfield, O. Oyerinde, B. Tebo, T. Spiro, *J. Biol. Inorg. Chem.* **2012**, *17*, 1151–1158; b) C. N. Butterfield, A. V. Soldatova, S.-W. Lee, T. G. Spiro, B. M. Tebo, *Proc. Natl. Acad. Sci. USA* **2013**, *110*, 11731–11735.
[12] J. J. Morgan, *Geochim. Cosmochim. Acta* **2005**, *69*, 35–48.
[13] a) L. G. van Waasbergen, M. Hildebrand, B. M. Tebo, *J. Bacteriol.* **1996**, *178*, 3517–3530; b) G. J. Dick, J. W. Torpey, T. J. Beveridge, B. M. Tebo, *Appl. Environ. Microbiol.* **2008**, *74*, 1527–1534.

↖↖ **These are not the final page numbers!**

[14] C. N. Butterfield, L. Tao, K. N. Chacón, T. G. Spiro, N. J. Blackburn, W. H. Casey, R. D. Britt, B. M. Tebo, *Biochim. Biophys. Acta Proteins Proteomics* **2015**, *1854*, 1853–1859.

[15] a) E. I. Solomon, U. M. Sundaram, T. E. Machonkin, *Chem. Rev.* **1996**, *96*, 2563–2606; b) E. I. Solomon, R. K. Szilagyi, S. DeBeer George, L. Basu-mallick, *Chem. Rev.* **2004**, *104*, 419–458.

[16] L. Quintanar, M. Gebhard, T.-P. Wang, D. J. Kosman, E. I. Solomon, *J. Am. Chem. Soc.* **2004**, *126*, 6579–6589.

[17] T. E. Machonkin, E. I. Solomon, *J. Am. Chem. Soc.* **2000**, *122*, 12547–12560.

[18] C. Stoj, D. J. Kosman, *FEBS Lett.* **2003**, *554*, 422–426.

[19] a) J. Su, P. Bao, T. Bai, L. Deng, H. Wu, F. Liu, J. He, *PLoS ONE* **2013**, *8*, e60573; b) J. Su, L. Deng, L. Huang, S. Guo, F. Liu, J. He, *Water Res.* **2014**, *56*, 304–313; c) L. Tao, T. A. Stich, C. N. Butterfield, C. A. Romano, T. G. Spiro, B. M. Tebo, W. H. Casey, R. D. Britt, *J. Am. Chem. Soc.* **2015**, *137*, 10563–10575.

[20] S.-K. Lee, S. D. George, W. E. Antholine, B. Hedman, K. O. Hodgson, E. I. Solomon, *J. Am. Chem. Soc.* **2002**, *124*, 6180–6193.

[21] a) E. I. Solomon, A. J. Augustine, J. Yoon, *Dalton Trans.* **2008**, 3921–3932; b) D. E. Heppner, C. H. Kjaergaard, E. I. Solomon, *J. Am. Chem. Soc.* **2013**, *135*, 12212–12215.

[22] a) D. L. Johnson, J. L. Thompson, S. M. Brinkmann, K. A. Schuller, L. L. Martin, *Biochemistry* **2003**, *42*, 10229–10237; b) S. Shleev, J. Tkac, A. Christenson, T. Ruzgas, A. I. Yaropolov, J. W. Whittaker, L. Gorton, *Biosens. Bioelectron.* **2005**, *20*, 2517–2554; c) S. Shleev, A. Christenson, V. Serezhenkov, D. Burbaev, A. Yaropolov, L. Gorton, T. Ruzgas, *Biochem. J.* **2005**, *385*, 745–754; d) A. Christenson, S. Shleev, N. Mano, A. Heller, L. Gorton, *Biochim. Biophys. Acta Bioenerg.* **2006**, *1757*, 1634–1641; e) Y. Kamitaka, S. Tsujimura, K. Kataoka, T. Sakurai, T. Ikeda, K. Kano, *J. Electroanal. Chem.* **2007**, *601*, 119–124; f) C. Léger, P. Bertrand, *Chem. Rev.* **2008**, *108*, 2379–2438; g) L. dos Santos, V. Climent, C. F. Blanford, F. A. Armstrong, *Phys. Chem. Chem. Phys.* **2010**, *12*, 13962–13974.

[23] a) J. A. Cracknell, K. A. Vincent, F. A. Armstrong, *Chem. Rev.* **2008**, *108*, 2439–2461; b) C. F. Blanford, C. E. Foster, R. S. Heath, F. A. Armstrong, *Faraday Discuss.* **2009**, *140*, 319–335.

[24] a) A. M. Bond, D. Elton, S.-X. Guo, G. F. Kennedy, E. Mashkina, A. N. Simonov, J. Zhang, *Electrochem. Commun.* **2015**, *57*, 78–83; b) A. N. Simonov, J. K. Holien, J. C. I. Yeung, A. D. Nguyen, C. J. Corbin, J. Zheng, V. L. Kuznetsov, R. J. Auchus, A. J. Conley, A. M. Bond, M. W. Parker, R. J. Rodgers, L. L. Martin, *PLoS ONE* **2015**, *10*, e0141252; c) H. Adamson, A. N. Simonov, M. Kierzek, R. A. Rothery, J. H. Weiner, A. M. Bond, A. Parkin, *Proc. Natl. Acad. Sci. USA* **2015**, *112*, 14506–14511; d) A. N. Simonov, W. Grosse, E. A. Mashkina, B. Bethwaite, J. Tan, D. Abramson, G. G. Wallace, S. E. Moulton, A. M. Bond, *Langmuir* **2014**, *30*, 3264–3273.

[25] D. Johannsmann in *Studies of Viscoelasticity with the QCM* (Eds.: A. Janshoff, C. Steinem), Springer, Berlin, Heidelberg, **2007**, pp. 49–109.

[26] K. A. Marx, *Biomacromolecules* **2003**, *4*, 1099–1120.

[27] A. M. Bond, E. A. Mashkina, A. N. Simonov in *A Critical Review of the Methods Available for Quantitative Evaluation of Electrode Kinetics at Stationary Macrodisk Electrodes*, Wiley, Chichester, **2014**, pp. 21–47.

[28] E. A. Mashkina, A. N. Simonov, A. M. Bond, *J. Electroanal. Chem.* **2014**, *732*, 86–92.

[29] M. C. Reed, A. Lieb, H. F. Nijhout, *BioEssays* **2010**, *32*, 422–429. K. A. Marx, *Biomacromolecules* **2003**, *4*, 1099–1120.

[30] A. Banh, V. Chavez, J. Doi, A. Nguyen, S. Hernandez, V. Ha, P. Jimenez, F. Espinoza, H. A. Johnson, *PLoS ONE* **2013**, *8*, e77835.

[31] A. M. Bond, N. W. Duffy, S.-X. Guo, J. Zhang, D. Elton, *Anal. Chem.* **2005**, *77*, 186A–195A.

[32] A. H. H. Tanji, F. Lima, S. R. Santos, G. Maia, *J. Phys. Chem. C* **2012**, *116*, 18857–18864.

[33] Z. Zhang, A.-E. F. Nassar, Z. Lu, J. B. Schenkman, J. F. Rusling, *J. Chem. Soc. Faraday Trans.* **1997**, *93*, 1769–1774.
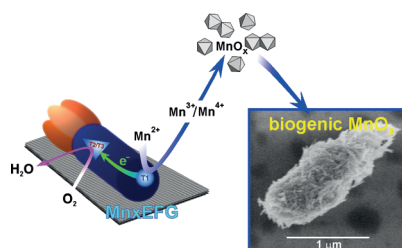
These are not the final page numbers! ↗↗

FULL PAPER

L. Tao, A. N. Simonov, C. A. Romano,
C. N. Butterfield, M. Fekete, B. M. Tebo,
A. M. Bond, L. Spiccia,* L. L. Martin,*
W. H. Casey*

■■ – ■■

Biogenic Manganese-Oxide Mineralization is Enhanced by an Oxidative Priming Mechanism for the Multi-Copper Oxidase, MnxEFG

In a natural geochemical cycle, manganese-oxide minerals (MnO$_x$) are principally formed through a diurnal microbial process, where a putative multicopper oxidase MnxG plays an essential role. Here, the kinetics of MnO$_x$ formation catalyzed by MnxEFG are examined using a quartz crystal microbalance, and the first electrochemical characterization of the MnxEFG complex is reported using Fourier-transformed alternating current voltammetry.

↖↖ These are not the final page numbers!